Astron. Astrophys. 321, 867–876 (1997)

ASTRONOMY AND ASTROPHYSICS

A study of the infrared spectrum of ψ Persei

I. A parameter study of the disc model

J.M. Marlborough[1], **J.-W. Zijlstra**[2], **and L.B.F.M. Waters**[3,4]

[1] Department of Physics and Astronomy, The University of Western Ontario, London, Ontario N6A 3K7, Canada
[2] Kapteyn Astronomical Institute, P.O. Box 800, 9700 AV Groningen, The Netherlands
[3] Astronomical Institute Anton Pannekoek, University of Amsterdam, Kruislaan 403, 1098 SJ Amsterdam, The Netherlands
[4] SRON Laboratory for Space Research Groningen, P.O. Box 800, 9700 AV Groningen, The Netherlands

Received 22 August 1996 / Accepted 18 November 1996

Abstract. We report a parameter study of emission lines arising from a disc surrounding a Be star, using parameters appropriate to the Be star ψ Per. We concentrate on the Hα line and on some IR recombination lines (Brα, Brγ, Pfγ and HI 17-6). The model we use is a simple cone-like disc model, first proposed by Waters (1986). This model has been successful in explaining the continuum energy distribution of Be stars, and we now wish to study the emission line spectrum emerging from such a disc. We find that line shapes and ratios of line strengths are strongly dependent on the temperature structure of the disc. Infrared recombination lines will therefore be very useful in determining the physical state of the circumstellar envelopes of Be stars.

Key words: stars: ψ Per; circumstellar matter; emission-line, Be – infrared: stars

1. Introduction

A Be star is a non-supergiant B star whose spectrum has, or has had at some earlier time, one or more Balmer lines in emission. Optical and infrared spectra of Be stars show emission lines, indicating the presence of cool, dense circumstellar envelopes. This material also produces excess free-bound and free-free radiation at optical and longer wavelengths. The underlying stars are rapid rotators, with vsini typically between 150 and 350 km/s. Observations in the ultraviolet reveal the presence of stellar winds of low density with high outflow speeds generally in the range 500 to 1000 km/s. All Be stars show irregular variations in all wavelength regions. More complete reviews of the properties of Be stars are given by Dachs (1987) and Underhill & Doazan (1982).

Recent interferometric data have demonstrated that the matter responsible for the Balmer emission lines and the continuum emission at radio wavelengths is not distributed with spherical symmetry (Dougherty & Taylor 1992; Quirrenbach et al 1994; Stee et al 1995). Instead the gas responsible for this emission has a much more disc-like distribution concentrated, perhaps strongly, to the equatorial plane. Many ad hoc models previously proposed for the distribution of the matter emitting this line and continuum radiation had assumed such a distribution (Marlborough 1987 and references therein). Two of these are the equatorially-concentrated, disc-like wind model (the PM model) of Poeckert & Marlborough (1978a, hereafter PMI) and the equatorial disc model (the disc model) of Waters (1986).

The general character of these ad hoc models has recently received strong theoretical support. Bjorkman & Cassinelli (1993) have shown that, under certain restrictive assumptions, a radiation driven wind from the polar regions of a rapidly rotating star is deflected toward the equatorial plane. The part of the radiation driven wind near the equatorial plane is compressed, and this compressed, less rapidly expanding wind resembles qualitatively both the PM model and the disc model. Numerical calculations by Owocki et al.(1994) confirmed this general picture; however more recent work by Owocki et al. (1996) suggests that a wind-compressed disc is not formed in the case of a strong line, radiation-driven wind of the CAK type (Castor et al. 1975). Both the PM and the disc models postulate an equatorially concentrated disk.

The PM model is specified by a moderately large number of free parameters. PM used this model to interpret observations of the Be star γ Cas (B0 IV). In a subsequent paper Poeckert & Marlborough (1978b, hereafter PMII) investigated the influence of various choices for these parameters on the model for γ Cas. The disc model, in contrast, is specified by a small number of free parameters. The disc model has been used extensively to interpret continuum emission of hot stars from the near infrared to longer wavelengths (Dougherty *et al.* 1994, and references therein). Waters & Marlborough (1992) have predicted some infrared recombination line profiles for hydrogen using the disc model. However no extensive parameter study of both optical

Send offprint requests to: J.M. Marlborough

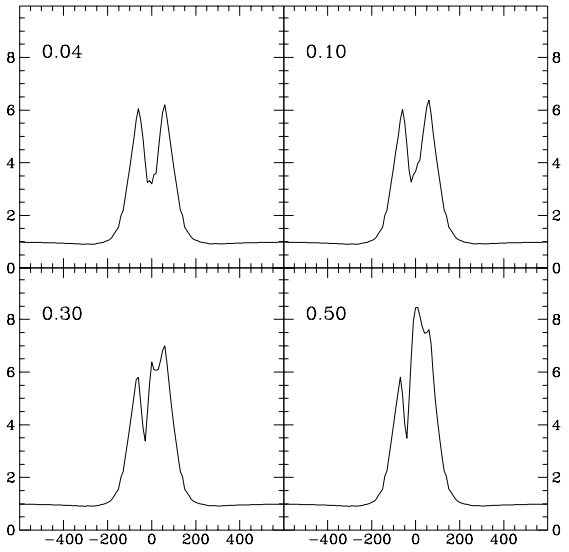

Fig. 1. The dependence of the strength and shape of Hα on the initial wind speed v_0. The ratio of v_0/a_0 is given in the upper left corner of each plot

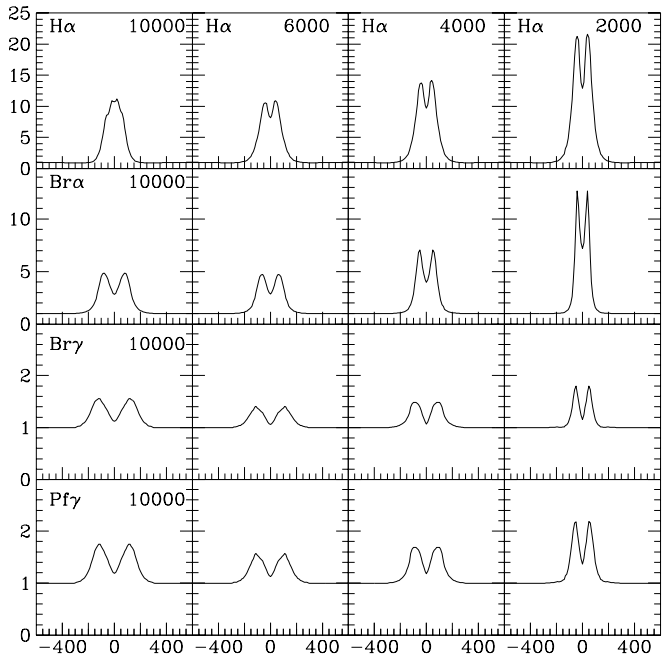

Fig. 2. The dependence of the profiles of Hα, Brα, Brγ, and Pfγ on disc temperature for the standard disc density. The temperature in K is given in the upper right corner of each box and is constant in a given column; the line identification is in the upper left corner. All profiles in a given row correspond to the same line

and infrared line profiles, analogous to that of PMII for optical lines and the continuum, has as yet been carried out for this model.

The infrared continuum and line spectrum can be used to put strong constraints on the structure and dynamics of Be star discs. The slope of the continuum is a sensitive indicator of the radial density and temperature gradients (e.g. Wright & Barlow 1975), while the recombination line spectrum in the IR is very rich and can be used to probe regions very close to the star (e.g. Waters & Marlborough 1992). The interplay between line and continuum opacity at long wavelengths allows us to draw conclusions concerning the geometry and the velocity field in the disc, conclusions that cannot be obtained using other methods. The infrared part of the spectrum will become more and more accessible as better spectrographs, both ground-based and space-borne, become available.

In this paper we investigate the effects of the various parameters of the disc model. We choose stellar parameters appropriate for the B5Ve star, ψ Per. In another paper we will present predictions, as a function of the wind temperature, of line profiles and line decrements for a selection of infrared lines. We will then attempt to find a consistent set of parameters for the disc model, which is capable of accounting for the observed profiles of Hα, Brα, Brγ, Pfγ and HI 17-6 in the spectrum of ψ Per.

2. The model

The basic parameters chosen for the star are summarized in Table 1. For the stellar parameters given in Table 1, the Keplerian orbital speed at the surface is 360 km/s. The star was assumed to rotate at 0.82 of this Keplerian orbital speed, so that $v_{\phi,0}$ = 295 km/s. This corresponds to a $v \sin i$ of 290 km/s at an inclination angle of 80°.

Table 1. The stellar parameters

$M_\star$	4.1 $M_\odot$
$R_\star$	6 $R_\odot$
T_{eff}	14500 K
$v_{\phi,0}$	295 km/s

The disc model is described by Waters (1986). We summarize the essential features here. The density $\rho(r)$ is given by

$$\rho(r) \; = \; \rho_0 (r/R_\star)^{-n} \cos^m \vartheta \qquad (1)$$

where $0 < \vartheta < \theta$, θ is the opening angle of the disc, ρ_0 is the wind density at the surface of the star, and $R_\star$ is the stellar radius. We chose as standard values: $\theta = 5°$, $n = 2.5$, $m = 0$, and a disc radius of 70 $R_\star$. In reality the disc is much larger than this (Dougherty & Taylor 1992); nevertheless, since the strength of the emission lines is proportional to density squared, these lines will be formed primarily in the inner part so that for the purpose of these calculations our choice of 70 $R_\star$ is sufficient. For a steady-state situation, the equation of continuity yields the velocity law

$$v(r) \; = \; v_0 (r/R_\star)^{n-2} \qquad (2)$$

where v_0 is the radial component of velocity at the surface of the star. We assumed Keplerian rotation in the disc, so that $v_\phi(r) = v_{\phi,0}\sqrt{(R_\star/r)}$.

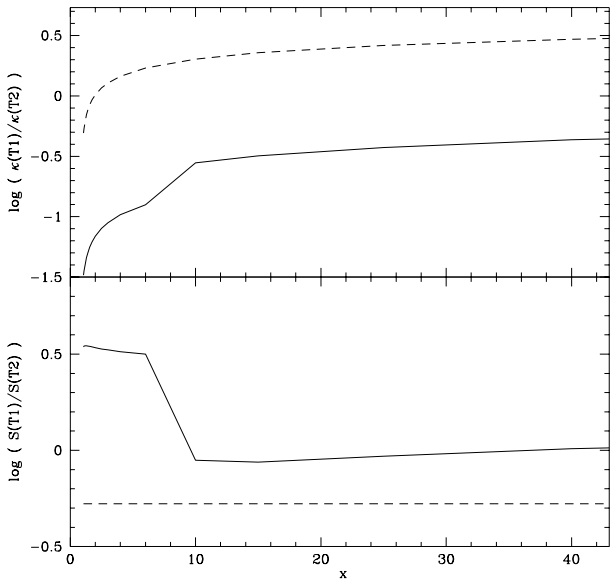

Fig. 3. The upper panel is the logarithm of the ratio of the volume absorption coefficient of the 6000 K model, κ_6, to that of the 10000 K model, κ_{10}, as a function of $x = r/R_\star$ in the equatorial plane of the disc; the lower panel is the logarithm of the source function ratio, S_6/S_{10}, as a function of x. The solid line is for Hα and the dashed line is for Brα. The apparent discontinuities reflect the finite number of points at which populations were determined

We assumed a pure hydrogen composition. Hydrogen line and continuum radiation, both of which vary as density squared, are produced in the disc. We neglected the emission from the fast, low-density wind seen in the UV (Lamers & Rogerson 1978). This is justified because the density in the fast wind decreases so rapidly with distance that it does not contribute significantly to the line or continuum flux. We considered both isothermal discs and discs having a temperature gradient proportional to $1/\sqrt{r}$.

The level populations of a five level H atom were determined using a modification of the method described by Waters & Marlborough (1992). Initially the electron number density, N_e, and the populations of levels 1 to 5 were determined as described in PMI. The Hα line profile was computed using these populations. However, for the infrared lines the populations of levels 4 and higher were obtained from the Saha-Boltzmann equation using the already determined N_e and the kinetic temperature T. The line profiles were calculated using a ray-tracing technique. For each line profile, several thousand lines of sight were used.

The basic parameters characterizing the disc model are given in Table 2. Our specific choice of standard disc parameters is simply a convenient set to produce an Hα profile which resembles generally that observed in ψ Per. The maximum disc radius is the maximum size of the disc in which we determined level populations. Unless stated otherwise we used the values from Table 2.

Table 2. The standard disc parameters

Initial wind velocity v_0	0.34 km/s
Isothermal sound speed a_0	8.5 km/s
(v_0/a_0)	0.04
Wind temperature	6000 K
Wind density ρ_0	2×10^{-12} g/cm^3
Inclination angle i	80°
Opening angle θ	5°
n	2.5
Maximum disc radius	70 $R_\star$
$v \sin i$	290 km/s

In subsequent sections we study how specific choices for each of the parameters of the disc model influence the shape and strength of Hα and some infrared recombination lines.

3. The initial wind speed

In Fig. 1 we show Hα line profiles for 4 values of the ratio v_0/a_0.

As expected the line becomes increasingly asymmetric as v_0/a_0 increases. The V/R ratio decreases from 0.98 at the smallest value of v_0/a_0 to 0.69 at the largest, where V and R represent, respectively, the intensities of the blue(V) and red(R) peaks of Hα. The equivalent width of the line increases with increasing v_0/a_0. Were the disc optically thin in Hα such an increase in equivalent width would not occur, because the increase in v_0 would simply shuffle emitting atoms in velocity space but not change the total energy emitted. Thus the disc must be optically thick in Hα (see also Sect. 8). Although the line emission from each fluid element remains the same, the increase in velocity lowers the probability of line absorption in the disc, thus yielding a stronger line.

We have deliberately chosen low values of the initial wind speed v_0. Specifically they are low compared to the value of 5 km/s used by Waters et al. (1987) in the disc model to interpret IRAS data for Be stars, and to the value of 7.5 km/s used by PMI in their model of γ Cas. These latter two values are undoubtedly much too large. PMI chose their tabular form of $v_r(r)$ to reproduce the asymmetric Hα line. However, PMII showed that 7.5 km/s was too large because, when the γ Cas model was viewed at inclination angles much closer to 90°, the Hα line had either a Type I or Type III P Cyg profile, decidely unlike the majority of Be stars (PMII, fig. 9).

The mass loss rate is given by

$$\dot{M} \;=\; 96.6\rho_0 v_0 R_\star^2 \sin\theta \qquad (3)$$

where $R_\star$ is in units of $R_\odot$, ρ_0 in g/cm^3, v_0 in km/s, and $\dot{M}$ in $M_\odot$/yr (Waters 1986). Using equation 3 and the data in Table 2, we obtain a mass loss rate $\dot{M}$ of 2.1×10^{-10} $M_\odot$/yr. In view of the sensitivity of the shape of the Hα profile to the ratio v_0/a_0, our $\dot{M}$ is the maximum possible consistent with a symmetric line.

It is also interesting to compare our $\dot{M}$ with other estimates. From an analysis of UV lines, Snow(1981) deduced mass loss

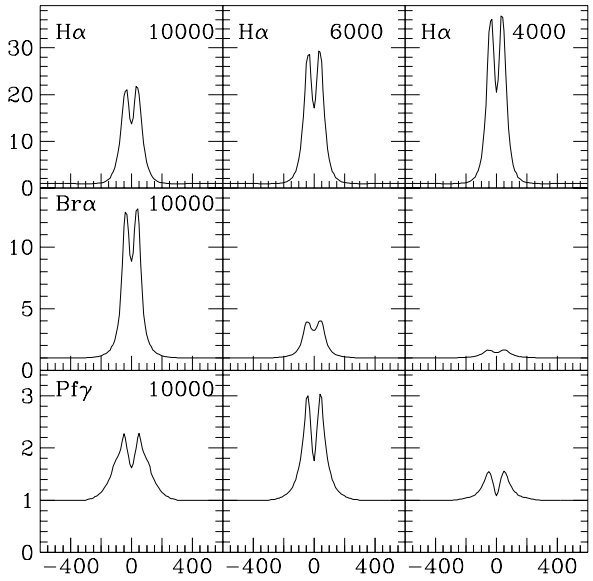

Fig. 4. The effect of a temperature gradient on the profiles of Hα, Brα, and Pfγ for the standard disc density. The temperature in K is given in the upper right corner and is constant in a given column. All profiles in a given row are for the same line

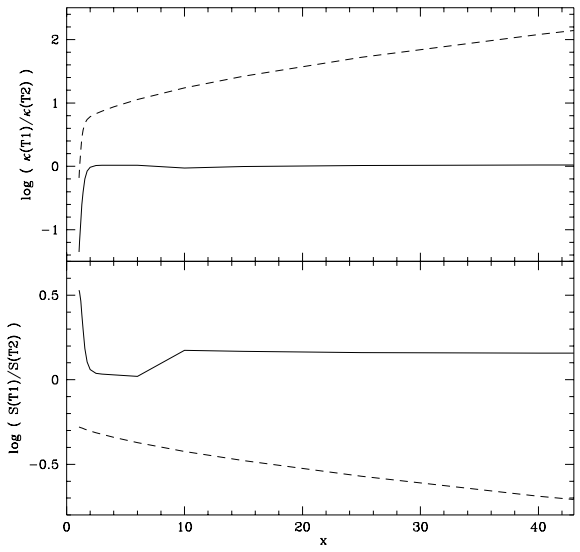

Fig. 5. The upper panel is the logarithm of the ratio of the volume absorption coefficient of the 6000 K model, κ_6, to that of the 10000 K model, κ_{10}, as a function of $x = r/R_\star$ in the equatorial plane of the disc; the lower panel is the logarithm of the source function ratio, S_6/S_{10}, as a function of x. The solid line is for Hα and the dashed line is for Brα. The apparent discontinuities reflect the finite number of points at which populations were determined

rates in the range 2×10^{-9} to 4×10^{-11} $M_\odot$/yr for 22 early to mid B stars, 19 of which are Be stars and one being ψ Per. For ψ Per Snow found $\dot{M}$ = $7.6\times10^{-11} M_\odot$/yr. Slettebak & Carpenter (1983) also found mass loss rates in the range 10^{-12} to 10^{-10} $M_\odot$/yr. The mass loss rates deduced from UV data are thought to refer to the lower density, polar wind. Thus at first glance the general agreement of the UV mass loss rates with our estimate based solely on the symmetry of Hα would seem to suggest that the mass loss rates in the polar and equatorial regions are similar, perhaps even the same. However, given the uncertainties present in the determination of mass loss rates from UV data and the arbitrary nature of our choice of the standard disc parameters in Table 2, this similarity may be simply fortuitous.

4. The disc (wind) temperature

We remind the reader that the density structure of the model is independent of the temperature of the wind. However a change in the temperature of the disc produces a change in the isothermal sound speed in the wind, thus yielding a different initial wind speed and a different mass loss rate compared to the standard model.

We have investigated the temperature dependence of the profiles of several recombination lines of hydrogen for two choices of T(r): a constant disc temperature and a temperature decreasing with r as $1/\sqrt{r}$. Neither may be realistic in practise but they do provide a sufficient range to illustrate how the various recombination lines depend on the actual disc temperature in the region in which they are formed. In our model the ionization equilibrium arises from the competing processes of photoionization by the geometrically and physically diluted photospheric radiation field and recombination at the local electron temperature. We assume this applies to the discs of Be stars, since we are unaware of compelling evidence for the existence of significant non-radiative heating in the disc. Non-radiative heating does occur in the Bjorkman-Cassinelli model, and in the calculations of Owocki et al. (1994), due to the supersonic collision of the equatorial wind with the equatorially deflected, polar wind, leading to highly ionized species such as N V, C IV, etc. High energy photons arising as a byproduct of this collision are not expected to influence significantly the ionization of hydrogen in the disc however, because of the small number of such photons and their low efficiency to photoionize hydrogen.

Consider first levels 1 to 3, whose populations are obtained from the solution of the statistical equilibrium equations. If the population, N_n, of one of these levels were determined only by the balance between photoionization from and recombination to that level, then N_n = N_e^2 α_n / B_n, where N_e is the local electron number density, B_n is the photoionization rate per particle in level n, and α_n is the recombination rate coefficient to level n. The temperature dependence of α_n is roughly $T^{-1/2}$ (Osterbrock 1974). Although radiative and collisional transitions between bound levels will also modify N_n, photoionization and radiative recombination are usually larger and thus the temperature dependence of α_n will have a major influence on N_n. In principle both the free-free and free-bound continua, j_ν(T), which vary as $T^{-1/2}$exp(-aν/T) where a is a constant and ν is the frequency, may influence the strength of Hα. For simplicity we have neglected the weak ν and T dependence of the free-free

Gaunt factor. Likewise Paschen continuum emission may also affect the strength of Hα. However, for all models considered here the effect of the free-free and free-bound continua on Hα is generally small.

As previously mentioned the populations of levels 4 and higher were assumed to be given by the combined Boltzmann-Saha equation, using the local values of N_e and T. Thus the source function for transitions between these levels is the Planck function. For a lower level of principal quantum number $l \geq 4$, the volume absorption coefficient, κ_λ, is given by

$$\kappa_\lambda \sim (u^2 A_{ul} \lambda_{ul}^2) \left(N_e^2 T^{-3/2} \right) exp\left[(\chi - E_l)/kT \right]) \qquad (4)$$

where u is the principal quantum number of the upper level of the transition considered, A_{ul} is the Einstein coefficient for spontaneous emission, λ_{ul} is the wavelength, χ is the ionization energy of hydrogen, and E_l is the excitation energy of the lower level of the transition.

4.1. Constant disc temperature

We chose 4 disc temperatures: 2000, 4000, 6000, and 10000 K. For each we computed the line profiles of Hα (0.66μ), Brα (4.05μ), Brγ (2.16μ), and Pfγ (3.74μ). We do not include H 17-6 (3.75μ) here since it is too weak at the standard wind density. Our results for each are shown in Figure 2.

Consider first Hα. From Fig. 2 we see in general that with decreasing temperature the equivalent width, or the line to continuum ratio, of Hα increases, the depth of the central absorption increases, and the separation of the red and blue peaks remains essentially constant. With decreasing temperature the full width of the line at half maximum decreases, since more of the emission comes from the outer part of the disc where the rotational speed is smaller. The profile for 10000 K shows the beginnings of a narrower central emission structure, yielding at higher densities the so-called winebottle appearance or winebottle profile (Barker 1986); several Hα profiles in PMII show this narrow, central emission structure. Hα lines for the same temperature but higher densities show more fully developed winebottle profiles.

These profile changes arise from the different radial dependences of the volume absorption coefficient and the line source function in the various models; such changes, in turn, reflect the temperature dependence of both the recombination coefficient, $\sim T^{-1/2}$, and the collisional transition rates between bound levels. Consider first the Hα profiles for 10000 K and 6000 K. In the upper portion of Fig. 3 we plot the logarithm of the ratio of the Hα volume absorption coefficient of the 6000 K model, κ_6, to that of the 10000 K model, κ_{10}, as a function of $x = r/R_\star$ in the equatorial plane of the disc; in the lower section of Fig. 3 we plot the logarithm of the Hα source function ratio, S_6/S_{10}, for the same disc location. The subscripts on κ and S are the temperature in units of 10^3 K. From Fig. 3 we note that the $\kappa_6 < \kappa_{10}$ at all positions x in the equatorial plane.

The largest differences occur for $x \lesssim 3$ and the difference decreases with increasing x. The Hα source function S_T, where

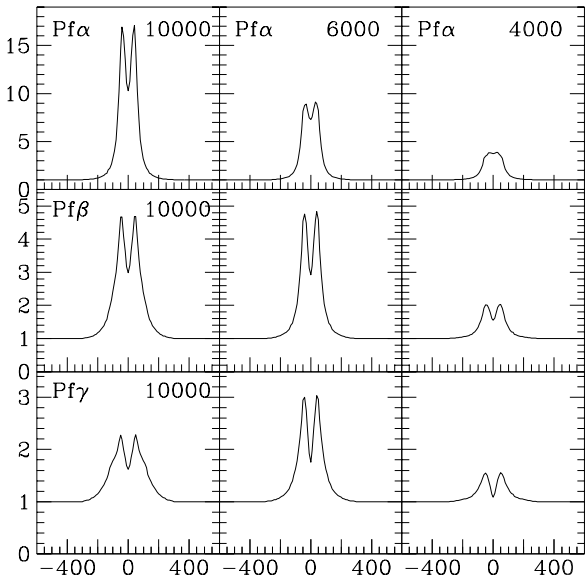

Fig. 6. The effect of a temperature gradient on on the line profiles of Pfα,Pfβ, and Pfγ for the standard density. The temperature in K is given in the upper right corner and is constant in each column; the line identification is given in the upper left corner and is the same in a given row

T is the disc temperature, behaves differently. For $x \lesssim 7$, $S_6 > S_{10}$, while $S_6 < S_{10}$ for $10 < x < 25$, and $S_6 > S_{10}$ for $x > 25$. Thus close to the star where the rotational speed is large, the source function and opacity changes yield stronger emission in the line wing for the 6000 K model compared to the 10000 K model. This enhanced emission in the line wing can be seen in the Hα profiles in Fig. 2 by comparing the profile heights at a velocity of 150-200 km/s. The double peak structure of the 6000 K profile occurs at a velocity of about $\pm$50 km/s. The symmetry of the profile suggests this is largely a rotational speed, the emitting gas being located at about $35R_\star$. As noted above $S_6 > S_{10}$ for such values of x.

Consider next the line profiles for 6000 K and 4000 K. For this pair of temperatures $S_4 > S_6$ at all x; the difference never is large but increases slowly with increasing x. Likewise κ_4 is marginally larger than κ_6 for all x. The larger line opacity also produces a weaker photospheric continuum at all locations in the disc; this also contributes to the increase in line strength at lower temperatures. The combined effect of all changes is a strengthening of the double peak structure, with little, if any, change in the line wings. Finally S_2 is slightly greater than S_4, the difference again increasing slowly with increasing x. The same comments apply to a comparison of κ_2 and κ_4. The Hα line is again stronger for the reasons mentioned above, but maintains a similar double peak structure.

The infrared lines display a range of behaviour which reflects changes in the line source function and the line opacity. Changes in the local continuum from free-bound and free-free emission contribute an additional variation, but this variation is never more than a few percent at most for the examples con-

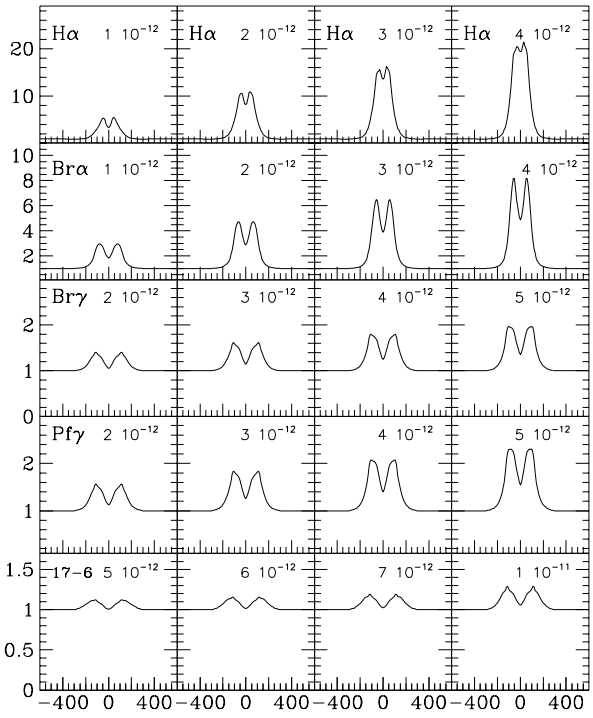

Fig. 7. The dependence of the profiles of Hα, Brα, Brγ, Pfγ and HI 17-6 on the disc density at the stellar surface for the constant standard disc temperature and the standard value of the density index n. The density is given in units of g cm^{-3}. The line identification is given in the upper left corner and is constant in a given row; the density is given in the upper right corner. Note the different range of density for some lines

sidered here. The line source function for all the IR lines is the Planck function, which decreases with decreasing temperature. The level populations of the infrared lines are given by the combined Boltzmann-Saha equation. Thus in addition to a dependence on the line strength and wavelength (equation 4), the line opacity will also depend on both the local electron temperature and the ionization-excitation equilibrium through the local electron number density.

Consider the Brα lines in the second row of Fig.2 for 10000 K and 6000 K. These two profiles are similar in appearance and strength. For the same line in discs with different temperatures T_L and T_H, where H is the higher and L the lower, we see from equation (4) that

$$\kappa_L/\kappa_H \sim [N_e(L)/N_e(H)]^2\ (T_H/T_L)^{1.5} \\ exp[D\,l^{-2}(T_L^{-1} - T_H^{-1})] \quad (5)$$

where D is a constant. The free electron number density is smaller everywhere in the lower temperature disc due to increased recombination at the lower temperature, and the ratio $N_e(L)/N_e(H)$ increases from 0.28 just above the stellar surface to 0.74 at $70R_*$. However each temperature dependent factor in equation (5) sufficiently exceeds unity so that $\kappa_6 < \kappa_{10}$ only for $x \lesssim 2$. For larger x, $\kappa_6 > \kappa_{10}$, and $S_6 < S_{10}$ for all x. Hence, between $x \simeq 1.1$ and the surface of the star the smaller value of the ratio κ_6/κ_{10} is sufficient to compensate partially for the smaller value of S_6/S_{10} so that some emission occurs in the far wings of the line. Beyond $x \simeq 1.1$, $\kappa_6 > \kappa_{10}$. Thus there is less emission from the outer regions with the result that the equivalent width of the 6000 K line is about 14% smaller than that of the 10000 K line.

The same behaviour continues from 6000 K to 4000 K to 2000 K. Comparing the 10000 K solution with the 4000 K and 2000 K solutions, one finds that the temperature dependent terms in equation (4) are now so large that there is no region close to the surface of the star where $\kappa_L/\kappa_H < S_L/S_H$, where (L,H) is the temperature pair (4,6) or (2,4), with the temperature expressed in units of 10^3 K. In particular, throughout the envelope the ratio $\kappa_4/\kappa_6 \simeq 4.6$ while S_4/S_6 = 0.56. Thus the smaller values of S_4 and S_2 mean less radiation, which would appear in the line wing, is emitted close to the surface of the star and the larger values of κ_4 and κ_2 imply that even less of this radiation escapes. Hence, with decreasing temperature each line becomes narrower at its base, the bulk of the line emission coming from the outer part of the disc where the rotation speed is small. Finally the local photospheric continuum at line center becomes progressively weaker with increasing line opacity. Thus the net effect of these variations is to produce a line to continuum ratio which increases with decreasing temperature.

Consider next Brγ in row 3 of Fig.2. The variation of the strength and shape of this line with decreasing temperature is qualitatively similar to that of Brα, although there is a larger decrease in strength from 10000 K to 6000 K and a smaller increase in strength to lower temperatures. The temperature dependent factors in equation (4) are the same for both lines since they have the same lower level l. Thus differences between the line shapes and strengths are due to the factor $(u^2 A_{ul} \lambda_{ul}^2)$ in equation (4). The ratio of this factor for Brγ compared to that for Brα is 0.063. Finally, since Brγ has a smaller wavelength and a smaller value of A_{ul}, the local photospheric continuum is not reduced to the same extent as it is at Brα. Hence there is a much smaller increase in line strength for Brγ with decreasing temperature below 6000 K.

The variation of Pfγ is illustrated in the last row of Figure 2. Both the lower and upper levels of this line are different compared to previous examples so that all factors in equation (4) will affect the line profile. Nevertheless, since Pfγ is intrinsically weaker than Brγ by a factor of 2.19, but its wavelength is larger by 1.73 though still smaller than that of Brα, one might expect the behaviour of Pfγ to be intermediate between that of Brα and Brγ, especially for temperatures below 6000 K. This expectation is confirmed by the variation shown in Fig.2.

4.2. Disc temperature with a radial gradient

We have also considered a wind temperature T varying as $1/\sqrt{r}$, with values at the star from 4000 to 10000 K. The profiles of Hα, Brα, and Pfγ for the standard density are shown in Fig. 4. We have not included Brγ because it shows essentially the same temperature dependence as Pfγ.

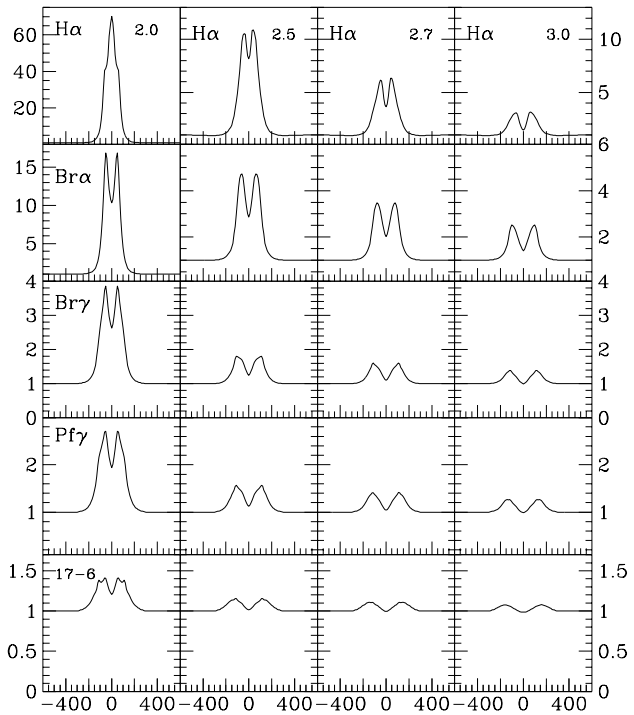

Fig. 8. The dependence of the line profile on the density index, n, for the constant standard disc temperature 6000 K. The value of n is given in the upper right corner of each box and is constant in a given column; the line identification is in the upper left hand corner of each box and is the same in a given row. The Hα and Brα profiles are for the standard wind density at the surface; the Brγ profiles are for a surface density of 4×10^{-12} gm cm^{-3} and the HI 17-6 profiles are for a surface density of 6×10^{-12} gm cm^{-3}. Note the different ordinate scales in the first two rows; in each case the ordinate scale of the profile on the left is different from the remaining three

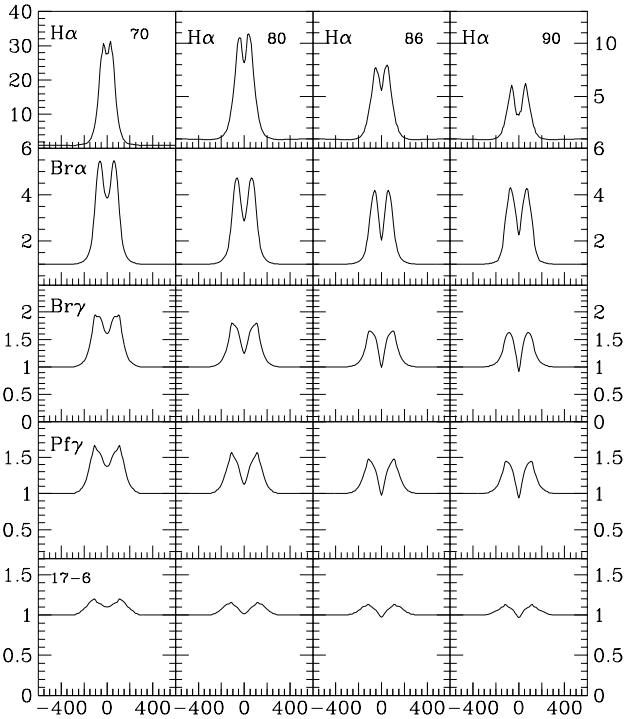

Fig. 9. The dependence of the line profiles for the standard model on the inclination of the observer's line of sight to the rotation axis. The line identification is given in the upper left corner and is the same for all boxes in a given row. The inclination angle, in degrees, is given in the upper right corner and is the same for all profiles in a given column. Note the different ordinate scales in the first row

It is clear from Fig. 4 that the three lines generally show dramatically different behaviour, first when compared with each other, and second when compared to the same line in Fig.2. This different behaviour arises from different relative combinations of the following physical effects: the atomic parameters of the particular line, the temperature dependence of the recombination coefficient, the temperature dependence of the line source function, the size of the region in which a given line forms, and the temperature gradient. Consider first Hα. Since it is an intrinsically strong line, it is formed over a large region of the disc. In this case because of the temperature gradient, the outer parts of each envelope are cooler than the same regions in envelopes of constant temperature and consequently recombination is enhanced above that occurring in the constant temperature disc with the same wind temperature at the surface of the star. Thus each Hα line in Fig. 4 is stronger than the corresponding one for the constant wind temperature case shown in Fig. 2.

Specifically, from Fig. 5 we see that for $x \lesssim 2.0$, $\kappa_6/\kappa_{10} < 1$ while $S_6/S_{10} > 1$. One aspect of this source function inequality is that more emission will occur in the wings of the line in the 6000 K model, although it is not obvious in Fig.4 due to the scale of the plot. Beyond $x \simeq 10$, $S_6/S_{10} \simeq 1.5$ while $\kappa_6 \simeq \kappa_{10}$. Therefore more emission arises in the outer parts of the 6000 K disc than in the hotter one. Comparing the 6000 K and 4000 K solutions one notes that except for a small region near $x \simeq 10$, κ_4 is at most only slightly greater than κ_6. Likewise S_4 is only slightly greater than S_6 inside $x \simeq 6-8$ so there is little, if any, change to the wings of the Hα line. However for $x > 10$, $S_4/S_6 \simeq 1.3$, so there is more line emission from the outer part of the disc where the rotation speed is smaller. Because of the slightly larger value of κ_4, the photospheric continuum at line centre in the outer part of the disc is somewhat smaller than it is for the 6000 K solution; this effect also contributes to increasing the line strength. The 4000 K line is thus stronger and has a somewhat smaller peak separation than the 6000 K profile. This latter aspect is not obvious, however, given the scale of the profiles in Fig.4.

In contrast Brα varies exactly opposite to Hα. Recall the source function for the infrared lines is the Planck function which decreases with decreasing temperature at a fixed wavelength. There are two explicit temperature dependent factors in equation (4); in addition to these, N_e depends implicitly on temperature. As a result of the assumed form for T(r), equation (5) becomes

$$\kappa_L/\kappa_H \sim [N_e(L)/N_e(H)]^2 (T_H/T_L)^{1.5}$$

$$exp[D\,l^{-2}(T_L^{-1} - T_H^{-1})\,r^{0.5}] \quad (6)$$

where T_L and T_H are, respectively, the temperatures in the disc at the surface of the star for the low temperature (L) and high temperature (H) discs. Thus κ_L/κ_H now has an explicit r dependence, together with a dependence on the lower level quantum number l.

Brα is the strongest infrared line considered here and therefore the strength and shape of its line profile will be influenced by conditions over a region of the disc which is larger than that for any of the other infrared lines. Because of the distance dependent temperature in the exponential term in equation (4), κ_λ will eventually increase with increasing distance from the star. The source function, the Planck function for the infrared lines, will decrease with increasing distance. Intrinsically weaker lines will therefore be influenced more by the physical conditions closer to the surface of the star.

From Fig.5 we see that the ratio S_6/S_{10} for Brα decreases continuously from 0.53 at the surface of the star; $S_6/S_{10} = 0.14$ at x = 65. In contrast κ_6/κ_{10} increases continuously from 0.66 to 364 over the same range of x, ultimately the result of increasing lower level populations with decreasing temperature. Thus Brα for 6000 K is significantly weaker than the same line at 10000 K. This same trend continues to 4000 K with $\kappa_4/\kappa_6 > \kappa_6/\kappa_{10}$ and $S_4/S_6 \simeq S_6/S_{10}$ for the same range of x. Thus Brα(4000) is again significantly weaker than the same line at 6000 K.

The Pfγ line initially increases in strength with decreasing temperature but eventually begins to decrease in strength as temperature continues to decrease. Pfγ is an intrinsically weaker line than Brα and thus its profile and strength will be influenced more by conditions closer to the surface of the star. The ratio of the term $(u^2 A_{ul} \lambda_{ul}^2)$ in equation (4) for Pfγ compared to that for Brα is about 0.1. The source function is larger for Pfγ than for Brα. One consequence of this is that more line emission is produced near the surface of the star where the rotation speed is significant. Because of the lower opacity more of this radiation escapes compared to that for Brα. It is clear from Fig.4 that Pfγ is significantly wider at its base than is Brα. A comparison of the 6000 K and 10000 K solutions shows that κ_6/κ_{10} increases rapidly from 0.5 just above the surface of the star to approximately 4 at x = 2, and continues to increase at a smaller rate to about 60 at x = 70. The ratio S_6/S_{10} behaves almost exactly the same as that for Brα. Because of the rapid increase in κ_6/κ_{10} near the surface of the star the profile for 6000 K is narrower at its base than it is for the 10000 K line. However the overall increase of κ_6/κ_{10} with x is smaller for Pfγ than for Brα because of the larger value of l^2 in the exponential term in equation (6). The source function variation is comparable for both lines. Thus, overall, the Pfγ line increases in strength from 10000 K to 6000 K, whereas Brα decreased in strength over the same temperature range. The Pfγ line is weaker in the 4000 K disc because the source function is smaller and the lower temperature more than compensates for the larger value of l^2 in equation (6). The combination of a smaller source function and a larger absorption coefficient yields a significantly weaker line.

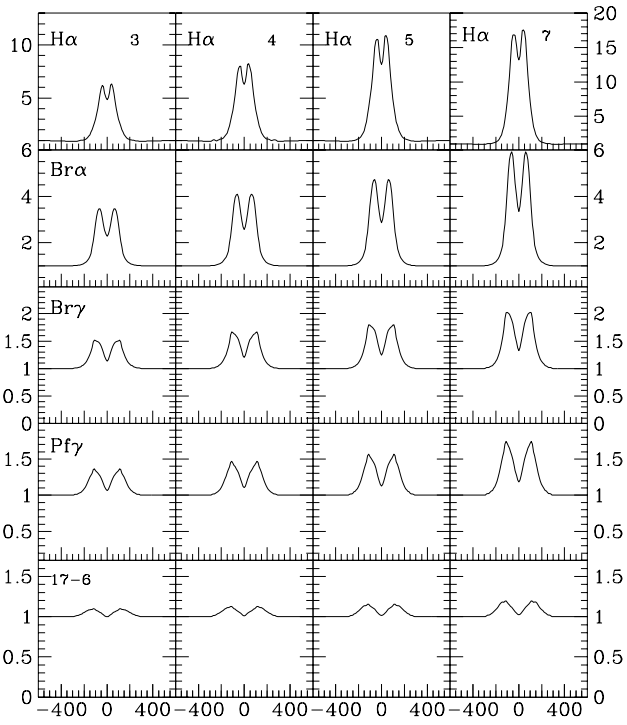

Fig. 10. The dependence of the line profiles on the disc opening angle, θ, for the standard disc model. The value of θ is given in the upper right corner and is the same for all profiles in a given column; the line identification in the upper left corner and is the same for all profiles in a given row. The Hα and Brα profiles are for the standard disc density, the Brγ profiles are for a density of 4 x 10^{-12} gm cm^{-3} and the HI 17-6 profiles are for a density of 6 x 10^{-12} gm cm^{-3}. Note the different ordinate scales in the first row

In Fig. 6 we compare the Pfα, Pfβ and Pfγ lines in order to show how the profiles of lines of a given series, which have the same lower level but different atomic parameters, can vary differently with temperature in the presence of a temperature gradient.

Pfα decreases continuously in strength with decreasing wind temperature at the surface of the star. Its variation is qualitatively similar to that of Brα in row 2 of Fig.4. Although A_{ul} for Brα exceeds that for Pfα by about 2.6, the term $(u^2 A_{ul} \lambda_{ul}^2)$ in equation (4) is larger for Pfα. Thus κ_λ is larger for Pfα. However each Pfα line is stronger than Brα for the same wind temperature. Thus the additional absorption must reduce the local photospheric continuum sufficiently to more than compensate for the smaller Pfα source function.

In contrast to Pfα the Pfβ line profiles for 10000 K and 6000 K are very similar in strength, while those of the Pfγ vary oppositely to Pfα. Since Pfβ is intrinsically weaker than Pfα, its profile will be representative of physical conditions in a region of the disc which is both smaller and closer to the surface of the star than is the corresponding volume for Pfα. A similar statement applies to Pfγ. The term $(u^2 A_{ul} \lambda_{ul}^2)$ is about a factor of 6 smaller for Pfβ than for Pfα, and decreases by an additional factor of 2.8 for Pfγ. The ratio of the Pfβ source function to

that for Pfα is approximately 1.6 for the range of temperatures in Fig.6. Thus both the larger source function and the smaller value of κ_λ very close to the surface of the star yield a Pfβ line, whose strength at 6000 K is very similar to that at 10000 K. At lower temperature the line weakens dramatically due to both the decreasing source function and increased opacity. The detailed behaviour of Pfγ has already been discussed.

Consider next the profiles in a particular column. The source function increases from Pfα to Pfγ due to the deceasing wavelength of each successive line. However the term $(u^2 A_{ul} \lambda_{ul}^2)$, and thus the opacity κ_λ, decreases from Pfα to Pfγ. Therefore a larger fraction of the radiation produced closer to the stellar surface can escape, leading to broader lines for increasing upper level quantum number u. This broadening is obvious in column 1 of Fig.6. Lastly note, as expected, that the Pfund line decrement, Pfn/Pfβ, is temperature dependent.

5. The disc (wind) density

In this section we consider how the choice of surface density and the density index, n, affect the line profiles of the various lines.

5.1. Surface density variations at constant disc temperature

In Fig. 7 we demonstrate how the choice of surface density of the wind affects the shape of various line profiles for the case that the wind temperature is constant at the standard value.

In general, all lines increase in strength with increasing density. For Hα the central absorption and the line width both decrease with increasing density, because of larger contributions to the profile from the outer parts of the disc. The infrared lines in contrast are formed closer to the surface of the star. They increase in strength with increasing density but generally have a smaller decrease in separation of the line peaks than does Hα.

5.2. Variation of the disc density gradient n at constant disc temperature

Both the density distribution and the velocity distribution depend on the density index n. Hence the profiles of lines formed in the disc will also depend on the density index n. In Fig. 8 we show profiles for the five lines at the standard disc temperature for a variety of values of the index n.

The numerical value of n affects the profiles in several ways. The larger is n, the more rapidly does the density decrease with increasing r, and the more rapidly does the radial component of velocity in the disc increase. It is clear from each row that the larger is n, the weaker is each line and the larger is the separation of the double emission peaks. At large n the bulk of the line is formed close to the star where the rotational component of velocity is large, thus yielding weaker lines with larger peak separations. As n decreases, the outer parts of the disc make a greater contribution to the line profile, and double peaks tend to be not as widely separated since the rotational speed decreases with increasing distance from the star. A larger r component

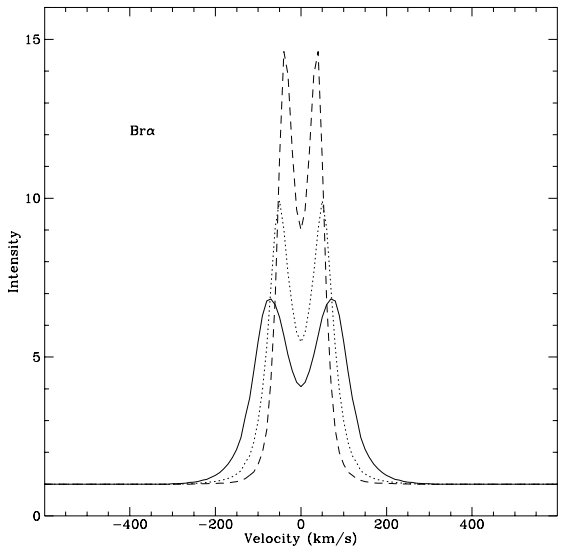

Fig. 11. The effect of the temperature on the line profile for the Brα line. The surface density is $3.0x10^{-12} gm/cm^3$. The solid line is for T = 10000 K, the dotted line for 4000 K and the dashed line for 2000 K. All other parameters have their standard values

of velocity would also lead to line asymmetries. Small asymmetries are present in Hα, but not in the infrared lines. Larger asymmetries are not seen in Hα due to the small initial wind speed used.

The Hα profile for n = 2 at the standard inclination of 80° shows the winebottle shape (Barker 1986). PMII found some profiles of similar shape, but at lower inclination angles. Hummel and Dachs (1992) have shown such profile shapes arise automatically through broadening by non-coherent scattering in a differentially rotating disc. Hanuschik et al. (1988) concluded from observational data that this two component structure is less commonly found at larger inclination angles. Perhaps the disc models with n = 2 have higher densities than would normally be encountered in Be star discs. Alternately, the disc model we have used may contain too much material at large distances from the equatorial plane (van Kerkwijk et al 1995).

6. The inclination angle

The choice of inclination angle affects the orientation of the disc as seen by the observer. As the inclination angle increases, the length of lines of sight passing through the disc increases, and thus optical depths generally become larger. However with increasing inclination angle, the effective radiating surface generally will decrease. If the disc is everywhere optically thin, the line strength will be independent of the inclination angle. For an optically thick disc the line strength depends on the size of the effective emitting surface. In Fig. 9 we show how the profiles of the various lines depend on the inclination angle.

For Hα as the inclination angle decreases, the line strength increases, the line width decreases, and the central absorption decreases slightly. The increase in line strength is due to the larger effective radiating surface and also to the reduction in the

range of radial velocity at which line emission occurs. The slight decrease in the central absorption arises from the smaller column of material projected against the stellar disc. The infrared lines behave in a similar way, except for the fact that very little change in line width occurs.

7. The opening angle θ

The opening angle θ is the angle between the equatorial plane and either the upper or lower boundary of the disc. Waters (1986) used an opening angle of 15°. Bjorkman & Cassinelli (1993) concluded that 0.5° would be a better choice. Owocki et al. (1994) discovered that a range between 1° and 3° was more appropriate. In Fig. 10 we show line profiles for opening angles in the range 3° to 7°.

The volume of the disc increases as the opening angle increases. Lines which are intrinsically strong are formed throughout the entire disc and thus increase significantly in strength as the emitting volume of the disc increases. The Hα profiles in the first line of Fig. 10 show this effect clearly. An intrinsically weak line, such as HI 17-6, changes by a much smaller amount, however. Since it is intrinsically weak it is formed preferentially in the denser inner part of the disc, and the effective emitting volume of inner portion of the disc increases by a much smaller amount. The other lines have strengths intermediate between Hα and HI 17-6.

8. The optical thickness of the disc

Several aspects suggest these discs are optically thick in line radiation. We have already noted that the equivalent width of Hα increases with increasing v_0/a_0, suggesting the discs are optically thick in this line. In Fig. 11 we show the effect of the envelope temperature on the Brα profile.

It is clear from Fig. 11 that the line intensity decreases with increasing temperature, and that the line width increases with increasing temperature. This change in line width is due to the optical thickness of the disc. If the disc is optically thick the line strength in the line wings will be lower for lower temperatures because the source function decreases with decreasing temperature. Lastly the increase of line strength with decreasing inclination angle also demonstrates that the disc is optically thick.

9. Discussion

We have carried out a study for the disc model of the circumstellar region around a Be star, using stellar parameters appropriate to the B5Ve star, ψ Per. We have defined a standard disc model based on a specific set of the parameters characterizing the disc model and have computed the line profiles of Hα and the infrared lines Brα, Brγ, Pfγ, and HI 17-6 for this standard model. We then varied successively each of the parameters characterizing the disc model to determine the sensitivity of the line profiles of all five lines to the specific values of each of the disc parameters. We find that different lines behave differently as a function of model parameters. In particular the line shapes and line strength ratios depend strongly on the temperature structure. Therefore IR recombination lines provide powerful tools to determine the physical state of the circumstellar material. In a subsequent paper we will predict line profiles and line decrements for a selection of infrared lines and then we will use observations of Hα, Brα, Pfγ, and HI 17-6 in the spectrum of ψ Per in order to see whether one set of disc parameters can be found which will reproduce satisfactorily the observed line profiles. We also intend to apply our models to ISO spectra of Be star discs.

Acknowledgements. JMM acknowledges financial support from the Natural Sciences and Engineering Research Council of Canada. LBFMW acknowledges financial support from the Royal Netherlands Academy of Arts and Sciences. JMM and LBFMW acknowledge financial support from a NATO Collaborative Reserach Grant (CRG.941220). We thank the referee, K. Wood, for his comments on our paper.

References

Barker, P.K.: 1986, PASP 98, 44
Bjorkman, J.E., Cassinelli, J.P.: 1993, ApJ 409, 429
Castor, J. I., Abbott, D. C., Klein, R. I.: 1975, ApJ 195, 157
Dachs, J.: 1987, in IAU Colloquium 92, *Physics of Be Stars*, eds. A. Slettebak and T.P. Snow (Cambridge: Cambridge University Press), 149
Doazan, V., Thomas, R.: 1982, in *Be stars with and without Emission Lines,* ed A. Underhill and V. Doazan (NASA monograph series)
Dougherty, S.M., Taylor, A.R.: 1992, Nature 359, 807
Dougherty, S. M., Waters, L. B. F. M., Burki, G., Coté, J., Cramer, N., van Kerkwijk, M. H, Taylor, A. R.: 1994, A&A 290, 609
Hanuschik, R. W., Kozok, J. R., Kaiser, D.: 1988, A&A 189, 147
Hummel, W., Dachs, J.: 1992, A&A 262, L17
Lamers, H.J.G.L.M., Rogerson, J.B.: 1978, A&A 66, 417
Marlborough, J. M. 1987 IAU Coll 92, Physics of Be Stars, ed. A. Slettebak and T. P. Snow (Cambridge: Cambridge University Press), 316
Osterbrock, D. E.: 1974 *Astrophysics of Gaseous Nebulae* (San Francisco: W. H. Freeman and Company), p16 and table 2.1
Owocki, S, Cranmer, S. R., Blondin, J. M.: 1994, ApJ 424, 887
Owocki, S, Gayley, K., Cranmer, S. R.: 1996, BAAS, in press
Poeckert, R., Marlborough, J.M.: 1978a, ApJ 220, 940 (PMI)
Poeckert, R., Marlborough, J. M.: 1978b, ApJS 38, 229 (PMII)
Quirrenbach, A., Hummel, D. F., Buscher, J. T., Armstrong, D., Mozurkewich, D., Elias II, N. M.: 1994, ApJ 416, L25
Slettebak, A., Carpenter, K. G.: 1983, ApJS 53, 869
Snow, T. P.: 1981, ApJ 251, 139
Stee, Ph., de Araujo, F. X., Vakili, F., Mourard, D., Arnold, L., Bonneau, D., Morand, F., Tallon-Bosc, I.: 1995, A&A, 300, 219
Underhill, A. B., Doazan, V.: 1982 B Stars With And Without Emission Lines Washington: N.A.S.A. SP-465.
van Kerkwijk, M. H., Waters, L. B. F. M., Marlborough, J. M.: 1995, A&A, 300, 259
Waters, L.B.F.M.: 1986, A&A 162, 121
Waters, L.B.F.M., Coté, J., Lamers, H.J.G.L.M.: 1987, A&A 185, 206
Waters, L.B.F.M., Marlborough, J.M.: 1992, A&A 253, L25
Wright, A.E., Barlow, M.J.: 1975, MNRAS 170, 41

This article was processed by the author using Springer-Verlag LaTeX A&A style file *L-AA* version 3.